RSC Advances

ROYAL SOCIETY OF CHEMISTRY

www.rsc.org/advances

Preparation, Characterization and antifouling properties of Polyacrylonitrile/Polyurethane blend membranes for water purification

Swapna Rekha Panda and Sirshendu De*

Department of Chemical Engineering, Indian Institute of Technology, Kharagpur

* Corresponding author

E-mail: sde@che.iitkgp.ernet.in

Tel: + 91 – 3222 – 283926

Fax: +91 – 3222 - 255303

Abstract

Casting of flat sheet Polyacrylonitrile (PAN)/Polyurethane (PU) blend membranes was reported for the first time in this work. PU makes the membrane more porous. Ternary phase diagram indicates, addition of PU increases thermodynamic instability of the blend. The average pore size of the membrane increased from 11 nm to 18 nm for pure PAN and PAN/PU blend membranes. The membranes were characterized in terms of permeability, porosity, molecular weight cut-off (MWCO), contact angle, mechanical strength, scanning electron microscope (SEM), Atomic force microscope (AFM), Differential scanning calorimeter (DSC) and Fourier transform infrared spectroscopy (FTIR). AFM images indicated that the surface roughness of the membrane increased with concentration of PU. Addition of PU also imparted hydrophilicity to the membranes. FTIR and DSC measurements confirm polymer compatibility of PAN/PU blend. PAN/PU blend 70/30 membrane exhibited the maximum antifouling characteristic with 99% flux recovery ratio associated with complete removal of turbidities and organic matters.

Keywords: Polymer blend; polyurethane; polyacrylonitrile; ternary phase diagram; flux recovery ratio; flux decline ratio.

1.0 Introduction

Polyurethane (PU) is one of the most versatile, biocompatible, biodegradable and viscoelastic polymer having two alternating hard and soft segments.[1,2] The hard segment includes aliphatic or aromatic diisocyanates, diols or diamine chain extenders. The soft segment consists of dihydroxy or diamine terminated reactive oligomers such as, poly-ethers, poly-esters, poly-butadienes, poly-acrylates with varying molecular weight.[2] The intermolecular hydrogen bonding between hard crystalline and soft amorphous parts with carbamate (-NH-CO-O-) network offers resistance to pH and temperature conditions and makes PU a suitable material for membrane preparation.[3] Polyurethane membranes were used in pervaporation industries in separation of aliphatic hydrocarbons, water vapor permeability study, due to flexible permeability and diffusivity.[4-6] PU based membranes have been investigated for biomedical applications, drug delivery systems, antimicrobial property and antifouling study.[7-12] PU membranes with fillers like zeolite and silver doped fly ash were used for treating textile effluents and which showed the removal of arsenic along with microorganisms.[13,14] Fabrication and characterization of PU based membranes has been reported by other researchers.[15-17]

On the other hand, polyacrylonitrile (PAN) is considered to be a good polymer in membrane industry due to its commercial availability, good thermal stability, resistance against organic solvents, better chemical stability against chlorine, sodium hypochlorite, sodium hydroxide.[18-20] Despite of its brittleness in dry condition, PAN membranes are known as low fouling due to their hydrophilicity compared to polysulfone (PSF), polyethersulfone (PES), polyethylene (PE) and polypropylene (PP).[21]

Modification of membranes by polymer blending has long been a subject of intensive investigation in both industries and academia.[22] The key features of PU blended membranes reported in literature are summarized in Table 1.

Table 1 Summary of previous reports based on PU blended membranes for various applications.

Reference	Polymer (wt%)/solvent (wt%) /additive (wt%)/ Type of membrane	MWCO (kDa)/ avg. pore size (nm)	Specific water flux $l/m^2.h.bar$	Other characterization
Sivakumar et al. 1998 [23];	CA, CA/PU blend (17.5)/DMF 82.5/ CA/PU (85:15) blend/DMF	20-69/NA	4-28.5	Water content/SEM
1999 [24];	PVP (0-2.5)/ CA/PU (85:15) blend/DMF	> 69/4-4.5/ NA	7-46	
2000 [25].	PVP (2.5-7.5)/ Flat sheet	20-69, 69/ NA	7-62.5	
Malaisamy et al. 2002 [27]	PU/SPSF blend (17.5)/ DMF/PEG 600 (0-7.5)/ Flat sheet	19-150/NA 6-20/NA	0.9-57.5	Porosity/SEM.
Latha et al. 2005 [28]	PU/CPSF blend (17.5) DMF/PEG 600 (0-10)/ Flat sheet	NA/NA	5.3-54	Permeability/SEM
Yuan et al. 2007 [29]	PVDF/TPU blend (16) DMAc/ PVP K30 (0-10)/ Hollow fiber	NA/NA	9-440	Cloud point/ DSC/porosity crystallinity/SEM/ FTIR-ATR.
Amado et al. 2005 [30]	PU and PANI blend (10-20)/pTSA CSA/ Flat sheet	NA/NA	NA/NA	Swelling/electrical conductivity/TGA/ FTIR-ATR/SEM
Zavastin et al. 2010 [31]	PU/CA blend (8:7) Acetone/--/ Flat sheet	NA/860	NA/NA	Swelling/porosity/ thermal analysis/TGA /FTIR-ATR/SEM
Velu et al. 2011 [32]	PSF/PU blend (17.5) DMF, DMAc/--/ Flat sheet	NA/ 4.3-10.7	3.3-13.1	Porosity/water content/ pore size distribution
Wu et al.2013 [33]	PVDF/PU blend (10 wt%) DMAc/--/ Flat sheet	NA/NA	NA/NA	degree of swelling/ FTIR/SEM/different solvents
Present study	PAN/PU blend (20) DMF/----/ Flat sheet	4-130/3-20	7.5-140	Cloud point/ Phase diagram /permeability/ Contact angle/porosity/ mechanical property/ SEM/AFM/DSC/FTIR BET measurement/ Turbid water application

Sivakumar et al.,[23-25] showed that PU enhanced the pure water flux with the formation of macrovoids which in turn resulted into higher molecular weight cut-off (MWCO) in cellulose acetate (CA)/PU blend membranes. Nair et al.,[26] showed a compatible system from the morphological changes, whereas, glass transition temperature indicated semi compatible behavior with confirmed interpenetrating polymer networks (IPN) formation on the interpenetration of PU with polyacrylamide (PAM) network. The work of Malaisamy et al.,[27] suggested that increased sulfonated polysulfone (SPSF) concentration in the PU/SPSF blend enhanced the membrane pore size and MWCO as well. In addition, use of PEG additive also controls the morphology, permeation characteristics and selectivity of the blend membranes. Latha et al.,[28] indicated the pore size increased with increased concentration of carboxylated polysulfone (CPSF) in CPSF/PU blend and role of polyethylene glycol (PEG) 600 was crucial in alternating the structural characteristics of the blend membranes.

Yuan et al.,[29] showed the flux was enhanced with the addition of thermoplastic polyurethane (TPU) and crystallinity decreased in polyvinylidenefluoride (PVDF)/TPU blend. In addition, lower concentration of PVP < (3 wt%), in the blend acted as a pore enhancer and higher concentration of PVP (10 wt%) in the PVDF/TPU casting solution suppressed macrovoid formation. Amado et al.,[30] verified distinguished morphological difference with addition of polyaniline (PANI) in the PU/PANI blend with no significant improvement in transport and electrical properties of membranes with the use of additives like p-toluene sulfonic acid (pTSA) and camphor sulfonic acid (CSA). However, 10-20% increase in Zn extraction compared to the commercial Nafion 450 membrane was reported. Zavastin et al.,[31] reported successful application of PU/CA blend membranes in waste water treatment of textile industry. Velu et al.,[32] reported the effect of solvents and PU concentration in PSF/PU blend membrane. The flux and protein rejection were increased for the blend ultrafiltration (UF) membranes with dimethylacetamide (DMAc) compared to dimethylformamide (DMF) as a solvent. Wu et al.,[33] reported blended PVDF/PU membranes showing better pervaporation performance with respect to pure PU membranes during the phenol waste water treatment. Exploration of membrane based technology in blood purification therapy was reported by several authors in recent past.[34-36] Besides, better antifouling and antithrombotic properties using PES/PU composite membranes during

dialysis operation was carried out by Yin et al.[37] Recent report by Roy et al.,[38] showed that PSF/PVP/PEG blend membrane was found to have adequate cyctocompatibility and blood compatibility for hemodialysis operation.

From the above literature review, it is evident that use of hydrophilic polymer, PU as a blend in casting solution has been proved to be an effective means of improving the permeability and selectivity of ultrafiltration membranes. As observed from Table 1, there is no report available on performance of PAN/PU blend membranes. The present work is undertaken to fill this gap. Effect of PAN/PU blend ratio on membrane morphology, permeability, molecular weight cut-off (MWCO), hydrophilicity, porosity and mechanical strength were studied. The polymer compatibility was confirmed using Fourier Transform Infrared Spectroscopy (FTIR), spectral analysis and DSC (thermal analysis) measurements. Antifouling characteristic of the membrane was evaluated using filtration data of turbid water.

2.0 Experimental

2.1 Materials

PAN homopolymer with molecular weight 50 kDa was obtained from M/s, Technorbital Advanced Materials Pvt. Ltd., Kanpur, India and was used as base polymer. Polyurethane (PU) was obtained from M/s, Lubrozol, Gujarat, India. Solvent DMF was purchased from M/s, Merck (India) Ltd., Mumbai, India. PEG of average molecular weight 200 Da, 400 Da, 600 Da, 4 kDa, 20 kDa, 35 kDa were supplied by M/s, S. R. Ltd., Mumbai, India. Dextran (average molecular weight: 70 kDa) and PEG of average molecular weight 100 kDa, 200 kDa were procured from M/s, Sigma Chemicals and M/s, Aldrich Chemicals, USA, respectively. These neutral solutes were used to evaluate MWCO of the cast membranes. Distilled water was used as the non-solvent in the coagulation bath. All chemicals used were of analytical grade without further purification.

2.2 Ternary phase diagram

The ternary phase diagram was generated using cloud point data obtained from titration method.[39] Various polymer blends with different concentration were prepared in

DMF in a sealed conical flask. A homogenous polymer solution was obtained using magnetic stirring for 8 hr at 60 ^{0}C. For titration, distilled water with 0.05 ml accuracy was poured dropwise into the polymeric solution under continuous stirring at 30 ^{0}C. The dropwise addition of distilled water was continued till the whole solution became cloudy. It was kept for another 30 min to check whether the turbid solution turned clear. If the solution turned clear, more water was added till the persistence of cloudiness continues for 30 min. The weight of water was recorded for every composition to plot the cloud point curve.

2.3 Determination of casting solution viscosity

Viscosity of the polymer solution was measured using a rheometer (model: Physica MCR 301, supplied by M/s, Anton Parr, Austria). The temperature of the unit was maintained at 25 ^{0}C. Viscosity of the casting solution was determined in the range of 50-500 s^{-1} shear rate. The composition of casting solution and blend ratio of cast membrane are given in Table 2.

Table 2 Membrane composition, and casting conditions for PAN/PU blend membranes.

Membrane Blend: Membrane code	**Blend composition (w/w)** PAN (%)	PU (%)	**DMF (wt %)**	**Viscosity (Pa.s) at 298 ^{0}K (216 s^{-1} shear rate)**
PAN:100/0 (Control membrane)	100	0	80	23.5
PAN/PU: 90/10	90	10	80	21.4
PAN/PU: 80/20	80	20	80	17.8
PAN/PU: 70/30	70	30	80	13.4
PAN/PU: 60/40	60	40	80	8.84
PU	0	100	80	1.52

Total polymer concentration 20 wt%, gelation bath temperature=25±5 °C; casting temperature 25± 5 °C; solvent evaporation time 30 s.

2.4 Membrane Preparation

Pure PAN, PU and PAN/PU blend membranes were prepared in flat sheet by phase inversion method. Composition of the casting solution is given in Table 2. The steps involved in membrane fabrication are as follows. Fixed amount of polymer was added to DMF heated at 40 ^{0}C and dissolved by means of stirring with the help of a mechanical

stirrer for 6-8 hrs to ensure complete dissolution of the polymer. During stirring, the lid of the container was kept closed to prevent the loss of solvent due to evaporation. The prepared solution was kept still for few hours without stirring at room temperature to remove air bubbles. In the first step of casting of membranes, non-woven polyester fabric of thickness 118±22.8 µm (product number TNW006013, supplied by M/s, Hollytex Inc., New York, USA) was attached to a clean glass plate using adhesive tape. Polymer solution was cast on a non-woven polyester fabric using a casting knife with an adjustable thickness fixed at 200 µm. Uniform casting time was maintained for all the casting solutions. The whole composite was immediately immersed in a precipitation bath containing distilled water at room temperature to initiate the non-solvent induced phase separation. The membrane was allowed to be in the precipitation bath for 10 min and then, it was transferred to another container with fresh distilled water for 24 h to remove the excess solvent. After that, the membrane was ready to be tested.

2.5 Antifouling test of blend membranes with turbid water

The applicability of the blend membranes were tested with turbid water, of feed concentration 500 NTU. The feed sample was prepared by dissolving some amount of local mud in water followed by filtration with a cloth filter to remove the coarse particles. The experiments were conducted in a stirred continuous ultrafiltration cell, at 552 kPa. The details of the experimental set up are available.[40] The cumulative volume of permeate was noted with time of filtration. The permeate flux was then evaluated from the slope of cumulative volume versus time history. Steady state permeate samples were analyzed using a turbidity meter supplied by M/s, EI Products, Parwanoo, India (Model: 331). Absorption value of permeate sample was also measured using a UV-VIS spectrophotometer (Perkin Elmer, Connecticut, USA) at 254 nm for detecting the presence of humic acid content in water. Each experiment was repeated three times and the average value was reported.

Fouling is a major drawback of UF membranes that leads to flux decline accompanied with an unexpected reduction in overall efficiency and economic viability of the membranes. Antifouling characteristic of blended UF membranes were quantified with the help of two parameters i.e., flux recovery (FRR) and flux decline ratio.[41] Filtration by all the membranes was carried out for 1hr. Before taking out the experimental run with turbid

feed, pure water flux of respective membranes, were measured at 552 kPa. At the end of 1h the cell was emptied. The membrane and the cell were washed thoroughly with distilled water. After that, pure water flux of the membrane was measured again, which is denoted by J_{w1}. Flux recovery ratio (*FRR*) was calculated using the following equation.[41]

$$FRR = \left(\frac{j_{w1}}{j_w} \right) \times 100\% \quad (1)$$

Flux decline ratio (*FDR*) is defined as,

$$FDR = (1 - \frac{j_p^t}{j_p^0}) \times 100\% \quad (2)$$

where, j_p^0 and j_p^t are the initial flux and final permeate flux at the end of one hour, respectively. FDR value signifies the reduction in permeate flux during experiment. A good antifouling membrane has high FRR and low FDR.

2.6. Characterization of membranes

The following characterizations were performed for the prepared membranes.

2.6.1 Scanning Electron Micrograph (SEM)

SEM images were analyzed using a scanning electron microscope (supplied by JEOL, Japan, model ESM-5800). First, the membrane was cut into small pieces, dried using a filter paper, dipped in liquid nitrogen for 1 minute and then fractured. The fractured samples were dried under vacuum. The samples were gold sputtered and then mounted on sample pad to observe the cross section and top view of the membranes.

2.6.2 Membrane permeability

Measurement of membrane permeability was carried out in a batch cell.[40] Effective area of the membrane in the module was 34 cm^2. First, the cell was filled with 500 ml of distilled water and membranes were compacted at 690 kPa for 3 to 4 hours. The permeate flux was calculated by

$$J_w = \frac{Q}{\Delta t \times A} \quad (3)$$

where, Q is the volumetric flow rate of permeating water, A is effective membrane area, Δt is the sampling time. Next, the steady state permeate flux was noted at five values of transmembrane pressure drop. A plot of J_w with transmembrane pressure drop resulted into a straight line through the origin. From the slope of this curve, membrane permeability was estimated.

2.6.3 Porosity (ε) and contact angle (CA)

Membrane porosity was measured by the mass loss of wet membrane after drying. The membrane, soaked with distilled water was weighed after removing superficial water with filter paper. Then, the wet membrane was placed in an air-circulating oven at 60 °C for 24 h and then further dried in a vacuum oven before measuring the dry weight until a constant mass was obtained. From the two weights (wet sample weight, w_0 and dry sample weight, w_1), the porosity of the membranes were calculated using the following equation.[41]

$$\varepsilon = \frac{w_0 - w_1}{\rho_w A l} \times 100\% \quad (4)$$

where, ε is the membrane porosity, A is the membrane surface area, l is the membrane thickness and ρ_w is water density. The membrane porosity of each sample was measured three times and the average values were reported. The contact angle was measured by a Goniometer (supplied by Labline instrument, Mumbai, India, manufactured by Rame-Hart instrument Co., New Jersy, USA; model number: 200-F4) using sessile drop method. The contact angle was measured at six different locations of the membrane and the average value was reported.

2.6.4 Molecular weight cut off (MWCO) of the membrane

Solute rejection measurements were carried out in a stirred batch cell. Solutions were prepared of 10 kg/m^3 using different neutral solutes, namely, PEG of different molecular weights, 400 Da, 4 kDa, 6 kDa, 10 kDa, 20 kDa, 35 kDa, 100 kDa, 200 kDa and dextran 70 kDa. The experiments were conducted at 138 kPa pressure and at 2000 rpm. The

permeate samples were analyzed using a refractometer (Abbe type, supplied by M/s, Excel International Ltd., Kolkata). Rejection values were plotted against the molecular weight of solutes in a semi-logarithmic curve. Molecular weight corresponding to 90% rejection was estimated as MWCO of the membrane. After the experiment, membrane was thoroughly rinsed with distilled water and its original permeability was restored. The rejection was calculated using Eq. (5) given below

$$R = \left(1 - \frac{c_p}{c_f}\right) \times 100\% \quad (5)$$

where, C_f and C_p are the concentration of solute in feed and permeate, respectively.

2.6.5 Measurement of average pore size

The average pore radius of the membranes were evaluated using Eq. 6. In this method, MWCO data was used to find out the average pore radius of the membranes.[42]

$$r_s = 16.73 \times 10^{-3} (\mathrm{MW})^{0.557} \quad (6)$$

In the above equation, r_s is in nm. MW is in Da. The pore radius of all membrane sample were also determined by Brunauer–Emmett–Teller (*BET)* instrument supplied by Quantachrome instruments, Florida, USA (model no. AUTOSORB-1). The BET analysis was carried out and the average pore diameter of the membranes was determined by degassing the sample at 65 ^{0}C prior to the measurement.

2.6.6 Atomic force microscope (AFM)

Surface morphology of the membranes was investigated using an atomic force microscope (AFM); (Model 5100, Agilent Tech, USA). Membrane samples of size (1×1cm) were placed in a glass substrate and surface images were taken in a scan area of 5 micron square area. The surface roughness of each membrane sample was measured and was reported in terms of root mean square (RMS) roughness.

2.6.7 Fourier Transform Infrared Spectroscopy (FTIR) analysis

In order to investigate the chemical changes occurred between the original PAN and PU membrane, as well as hydrophilically modified PAN/PU blend membranes at different

blend ratios, FTIR (supplied by M/s, Perkin Elmer, Connecticut, USA; model: Spectrum 100) analysis was performed. The transmittance value at specific wavelength signifies the presence of the functional groups present in the respective membrane.

2.6.8 Differential scanning calorimetry

The thermal analysis of pure and blended membranes were carried out in a differential scanning calorimeter (procured from M/s, TA instrument Ltd., New castle, Delaware USA; model DSC Q_{20}). The whole experiment is carried out in a two step heating cooling cycle in nitrogen atmosphere. The analysis was carried out utilizing around 5 mg of membrane samples kept in an aluminum pan and heated from 0 to 350 ^{0}C at a heating rate of 10 ^{0}C/min.

2.6.9 Mechanical properties of membranes

Tensile strength, percentage elongation, elastic modulus of all cast membranes at were determined by a universal electronic strength measuring instrument (procured from M/s, Tinius Olsen Ltd., Redhill, England of model H50KS). Measurements were carried out at room temperature and at strain rate of 10 mm/min. The reported value was the average of at least five samples.

3. Results and discussions

3.1 Polymer-solvent-nonsolvent interaction

Two different polymers PAN, PU are used to prepare the PAN/PU blend membranes. Fig. 1(a) clearly shows the structure of these two polymers. The relative affinity of polymer and solvent can be estimated using Hansen solubility parameter denoted by δ which is described as the square of cohesive energy density given by Eq. (7)

$$\delta^2 = \delta_p^2 + \delta_h^2 + \delta_d^2 \quad (7)$$

δ includes a polar component due to dipole-dipole interactions (δ_p), hydrogen bonding forces component (δ_h) and a dispersive force component (δ_d).[43] The materials having similar values of Hansen solubility parameter δ, are likely to have higher miscibility. The difference

in the solubility parameter for polymer-solvent interaction can be calculated using the equation given below.[43]

$$\Delta\delta_t = \sqrt{(\delta_{P,p} - \delta_{S,p})^2 + (\delta_{P,h} - \delta_{S,h})^2 + (\delta_{P,d} - \delta_{S,d})^2} \quad (8)$$

where, symbols p, d, h indicates polar, dispersive and hydrogen bonding components, respectively and symbols P, and S denotes for "polymer" and "solvent" separately. The above equation can be used, to predict the relative affinity of solvent with the polymers for both the systems i.e., PAN/DMF and PU/DMF. Smaller is the value of $\Delta\delta_t$, stronger is the polymer-solvent interaction. The solubility parameters of polymers, solvent and non-solvent are listed in Table 3.[3] It was found that, the value of $\Delta\delta_t$ for PAN-DMF pair (4.84) is smaller than that of PU-DMF system (10.62). This indicates miscibility of PAN in DMF is better than that of PU. The hydrogen bonding component, δ_h value (Table 3) of PAN and PU are close to each other, suggesting possible formation of hydrogen bond between two polymers in the blend. Fig. 1(b) shows the possible H-bonding interaction between the functional groups of $(C \equiv N)$ in PAN and urethane group in polyurethane.

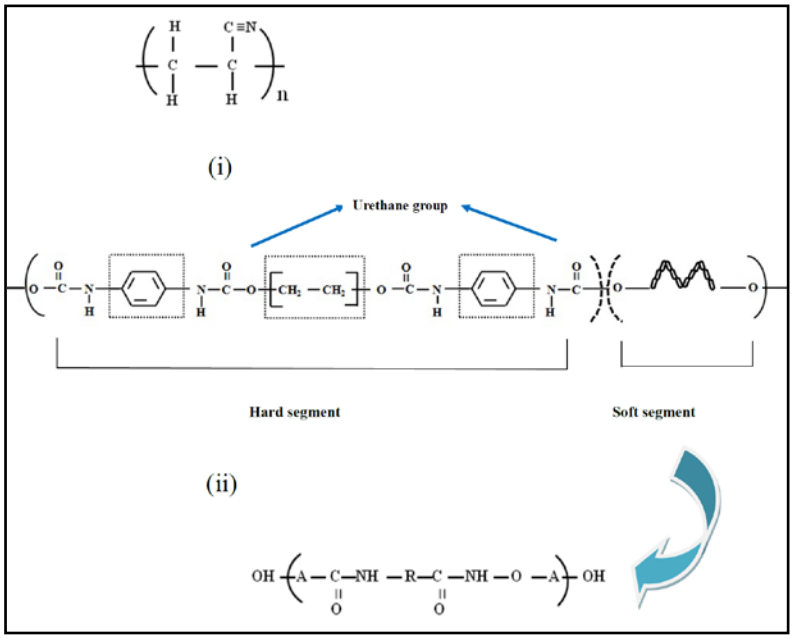

(a)

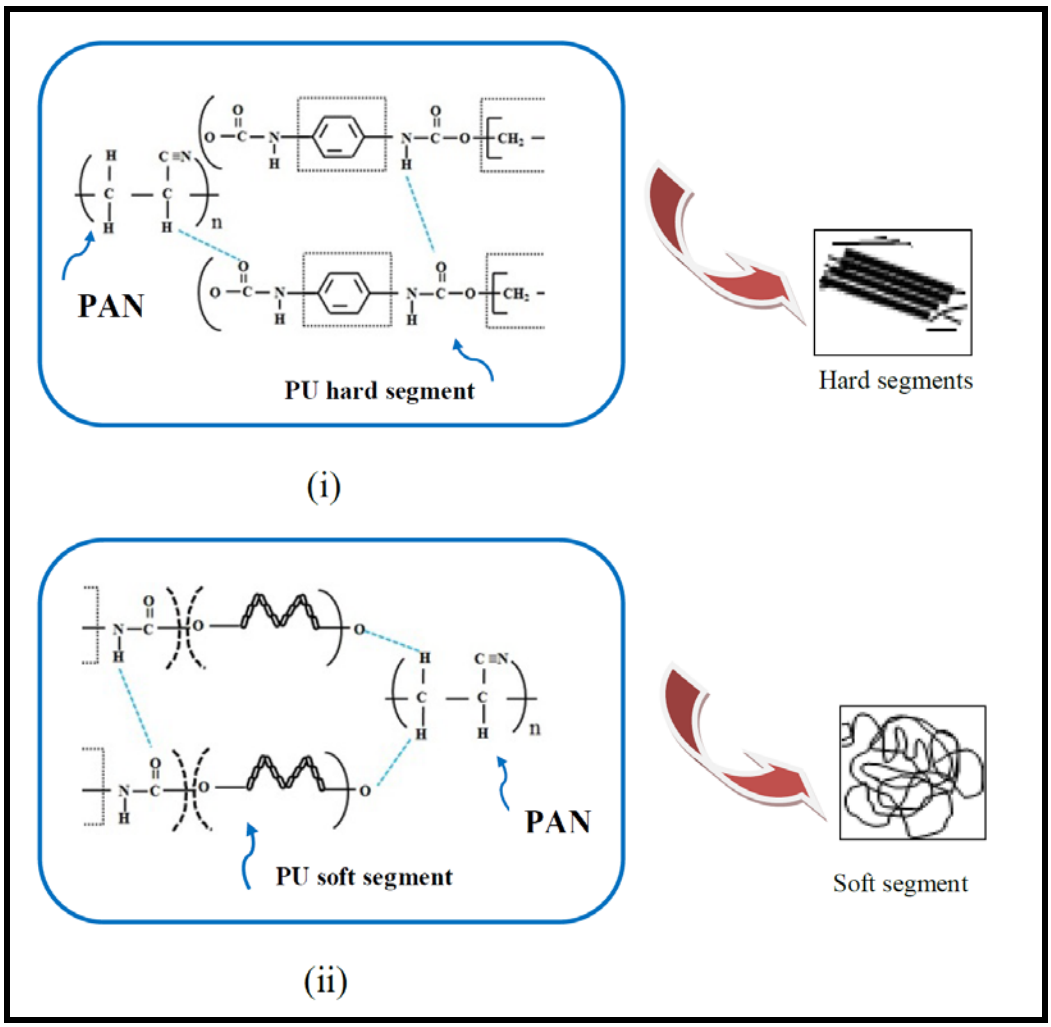

(b)

Fig. 1 Molecular structure of polymers are shown; (a) (i) Polyacrylonitrile (PAN); (ii) Polyurethane (PU); (b) Possible hydrogen (H) bonding in between PU chains and PAN polymer for blend membranes: (i) Between hard segments of PU with PAN; (ii) between soft segments of PU with PAN.

3.2 Viscosity of casting solution and ternary phase diagram

Viscosity of casting solution is a key factor for membrane formation during phase inversion process. It is believed that higher solution viscosity reduces the mobility of the polymeric chain during phase inversion, affecting the precipitation kinetics and thus the membrane morphology.[44] Total polymer concentration of all cast membranes was maintained at 20 wt%. The viscosity data shown in Table 2 reflects that (increasing the percentage of PU from 10% to 40%, in the PAN/PU blend), for various blend ratios 90/10 (10% PU), 80/20, (20% PU), 70/30 (30% PU) and 60/40 (40% PU), viscosity decreases due to viscoelastic and rubber like properties of PU polymer.[2-4] Highest viscosity is recorded for pure PAN polymer which is in agreement with the literature.[45]

The thermodynamic stability of the casting solution is interpreted using ternary phase diagram. The ternary diagram explains the polymer-solvent-nonsolvent interaction in a casting solution. The isothermal phase diagram of PAN/DMF/water, PU/DMF/water and PU-blend-PAN/DMF/water system is shown in Fig. 2.

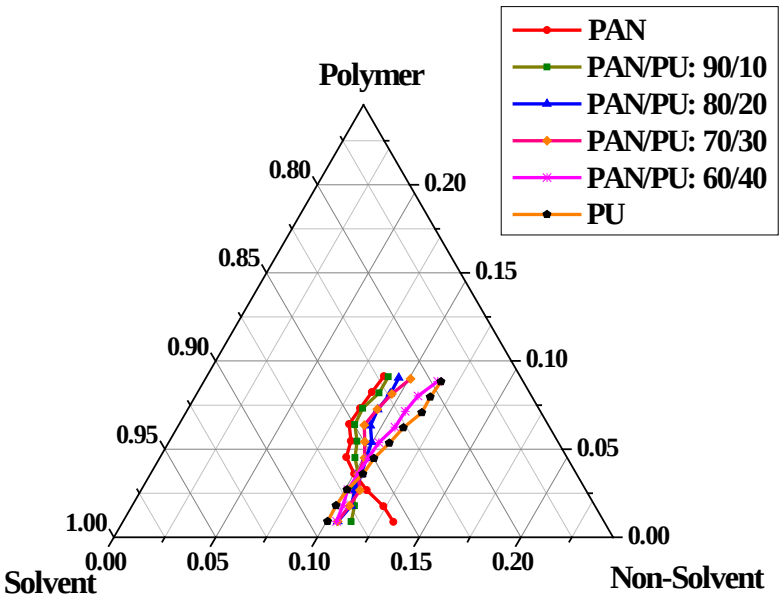

Fig. 2 Experimental cloud point data pure and PAN/PU blend polymers in polymer/DMF/water system.

The binodal curves for six cast membranes of different compositions were determined based on the cloud point measurement. Binodal curve in a ternary diagram divides the triangle into a homogenous single phase region and a non-homogenous two

phase region (solid-polymer rich phase, liquid-polymer lean phase).[46] It was observed from Fig. 2 that, the binodal concave curve shifts towards the polymer-solvent axis for PAN/DMF/water system. Hence, the system precipitation is reached by the addition of lower content of water. The present result is in agreement with the earlier report by Tan et al.[47] Addition of PU from 10% to 30%, shifts the binodal curve gradually towards right. Curvature of binodal curve decreases with concentration of PU in the blend and it finally becomes almost linear for pure PU. The curve resembles to pure PAN qualitatively upto 30% PU. However, further addition of PU (40% and above) reduces thermodynamic stability of the casting solution leading to a linear shaped binodal curve. It is interesting to note that viscosity of the casting solution is reduced with PU concentration. This may be due to poor interaction between PU and DMF as found from the solubility parameters (Table 3).

Table 3

[1]Solubility parameters $(MPa)^{1/2}$ of polymers, solvent and non-solvent.

Chemicals	δ_d	δ_p	δ_h	δ
PAN	21.70	14.10	9.1	27.43
PU	18.45	3.66	9.90	21.25
DMF	17.4	13.7	11.3	24.8
Water	15.5	16.0	42.3	47.8

[1]parameters of Table 3 are extracted from reference.[3]

Thus, DMF is a better solvent for PAN than PU. In a poor solvent, a rubbery elastic polymer like PU, the hard and soft segments of polymeric chain tend to attract each other, which may result to a loose unfavorable polymer-solvent interaction. The system becomes thermodynamically unstable, leading to instantaneous demixing and porous morphology.[44] Similar finding is available for pure PU-DMF system.[48]

3.3 Morphological study by SEM

SEM analysis is an important tool for the morphological characterization of membrane surface. It is a well known fact that, an asymmetric membrane consists of a top layer (skin layer), a middle layer (sub layer) and a small sponge like bottom surface layer. The skin layer acts as a separation layer. The support layer provides the mechanical strength. SEM images of individual and PAN/PU blend membranes are represented in Fig.

3. Left side column shows the cross sectional views, whereas top surface images are given in the right side column.

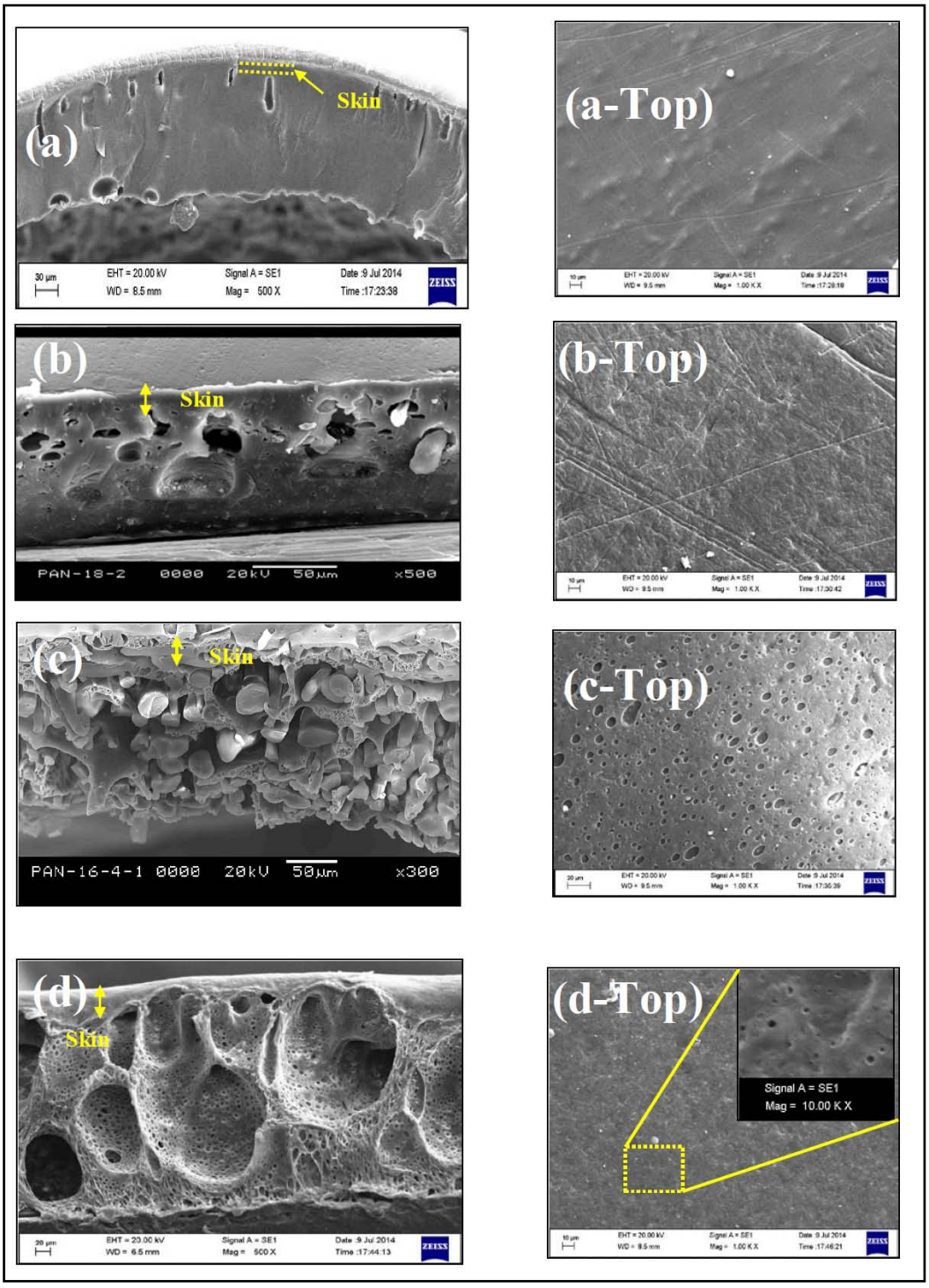

Fig. 3 Cross sectional and top view SEM images of pure and blended PAN/PU membranes (a) PAN (b) 90/10 (c) 80/20 (d) PU.

For higher PU% in the blend, at 70/30 and 60/40 PAN/PU blend ratios, SEM images are given in the supporting figure Fig. S1. Viscosity data in Table 2 shows a consistent decrease of polymer viscosity with PU concentration. For 20 wt% pure PAN, viscosity is the highest. Higher viscosity hinders demixing process that leads to denser skin layer which promotes selectivity (higher rejection) but lesser throughputs (permeate flux).[49] This observation is verified by a dense morphology (Fig. 3a), for pure PAN membrane. The top view SEM image (Fig. 3a-top) also supports the dense morphology for PAN membrane. Further increase of PU concentration in the blend from 10% to 40%, viscosity of the casting solution decreases. Thus, more non solvent penetrates into the membrane matrix as discussed in section 3.2 and Fig. 2. This leads to rapid demixing. Thus, both thermodynamic instability and kinetic hindrance control the membrane morphology. The combined effects, result to the formation of macrovoids in the membrane cross section with increasing concentration of PU in the blend (Figs. 3b, 3c and Fig. S1). The typical presence of macrovoids on the membrane morphology is associated with the formation of pores on the membrane top surface. In addition, SEM images for 90/10, 80/20 blend membranes have some clear visible open pores on their top surfaces. However, bigger pore size membranes are obtained at 70/30 and 60/40 blend ratios that support SEM images given in Fig. S1. Total membrane thickness and skin thickness of the cast membranes measured from SEM images are shown in Table 4.

Table 4 Effects of blend ratio on different morphological parameters of PAN/PU blend membranes.

Membrane code	**MWCO (kDa)**	**Comparison of membrane pore sizes (diameter)**		**Membrane thickness (µm)**	**Skin thickness (µm)**
		Eq. 4 (nm)	**BET (nm)**		
100/0 (PAN)	4	3.4	11.6	120	10
90/10	14	6.8	12.4	110	6.5
80/20	46	11.5	14.0	105	6
70/30	87	16.0	16.4	60	1
60/40	128	20.7	18.0	55	0.5

The data in Table 4 indicates membrane skin thickness decreases with PU concentration. Similar observation is reported by Malaisamy et al.,[27] in case of blending PU with PSF, by Sivakumar et al.,[23] for CA/PU blend and by Velu et al.,[33] for PSF/PU systems, respectively. SEM image of pure PU is given in Fig. 3(d). Pure PU having the least viscosity (Table 2), exchange of solvent-non solvent is augmented. Thus, spongy structures with plenty of pinholes are visualized in cross sectional SEM images. SEM images showed a thicker morphology for pure PU compared to other membranes. General trend describes membrane thickness is mostly altered by thermodynamic and kinetic behavior of the casting solution. Hence, higher kinetic instability gives rise to a thicker morphology.[50] In addition, shifting of binodal curve towards polymer-non solvent axis ensures an unstable system at 20 wt% pure PU concentration, as discussed in section 3.2. The overall thickness (140 μm) and skin thickness (12 μm) of pure PU membrane are also the highest. However, no pores are visible at the top view of this membrane at 1000X magnification. But, pores are seen at higher magnification of 10000X, indicating its spongy cross sectional morphology (Fig. 3d). Although the membrane seems to be porous, it offers more resistance against solvent flow due to larger thickness (overall and skin). Although, reports suggest that, pure PU membrane is generally applied for gas separation and solvent purification purposes rather water based separations.[51] Therefore, only PAN/PU blend membranes are characterized and examined for application for treatment of turbid water.

3.4 Membrane permeability

Permeation results of various cast membrane are presented in Fig. 4. From this figure, it is clear that pure PAN 100/0, control membrane has the least permeability of 1.84×10^{-11} m/Pa.s. With addition of PU in the blend (10% to 30%), permeability increases to 2.37×10^{-11} m/Pa.s (90/10), 5.14×10^{-11} (80/20) and 6.87×10^{-11} m/Pa.s (70/30), respectively.

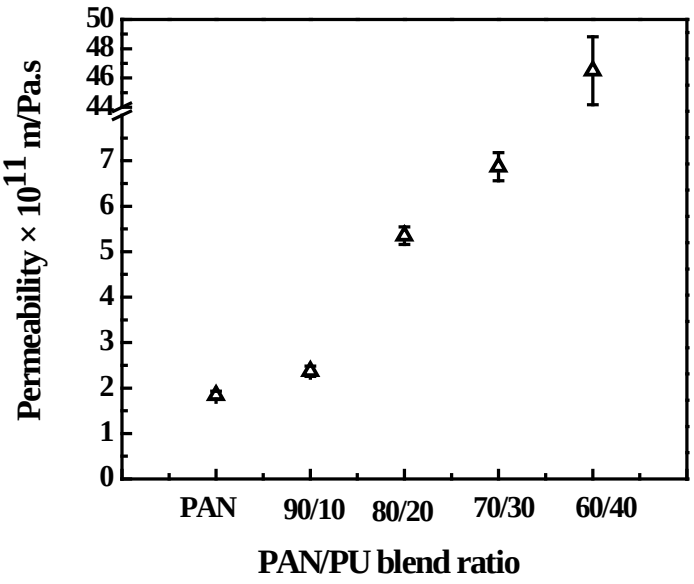

Fig. 4 Permeability of pure and PAN/PU blended membranes.

Further, increase of PU to 40% i.e., at (60/40) blend ratio, results in a significant increase of membrane permeability to 4.65×10^{-10} m/Pa.s. The data appropriately corroborate with SEM images (Fig. 3 and supporting figure, Fig. S1), described in section 3.3. Viscosity plays a major role in the demixing process. As viscosity decreases with PU concentration, the non solvent penetration in the membrane matrix is enhanced, that results to instantaneous demixing as discussed earlier. Instantaneous demixing is associated with loose and porous membrane structure. Hence, permeability shows an increasing trend with the addition of PU in the blend membranes. However, a drastic increase of membrane permeability for PAN/PU, 60/40 blend composition explains the formation of rougher membrane due to the elastic and rubbery behavior of PU polymer. Similar trend is reported earlier for increased PU concentration in CA/PU blend and TPU concentration in PVDF/TPU blend membranes.[23-25, 29]

3.5 Porosity and contact angle

Effect of PU, on porosity and contact angle of the cast membranes are shown in Fig. 5. It is observed that PAN/PU blend membranes at 90/10, 80/20, 70/30 and 60/40 blend ratios, showed an appreciable increase in membrane permeability compared to pure PAN and PU membranes.

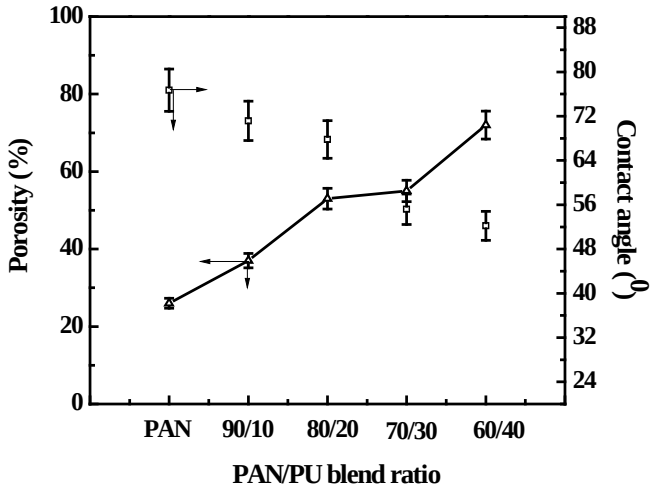

Fig. 5 Porosity and contact angle of pure and PAN/PU blended membranes.

Membrane porosity increased with PU concentration in the blend membranes. The results are in line with the SEM images shown in Fig. 3 that, the presence of bigger pores on the membrane surface results to a more permeable membrane. Similar type of observation was reported by Malaisamy et al.,[27] for PU/SPSF blend membranes. Addition of PU decreases the contact angle from 81^0 (PAN) to 72^0 (90/10), 69^0 (80/20), 56^0 (70/30) and 51^0 (60/40) for the said PAN/PU blend ratios, respectively. This indicates addition of PU could be a useful tool to improve membrane hydrophilicity. Permeability and porosity of the membranes increase with PU concentration and hence average value of contact angle (Fig. 5) shows an expected decreasing trend. Pure PAN exhibited the lowest porosity (25%) due to its dense morphology as shown in Fig. 3(a). The contact angle obtained for this membrane was 76^0. The results are in corroboration with the SEM images and permeability measurements, as discussed in preceding sections.

3.6 MWCO of membrane

The MWCO curves of all cast membranes were determined individually based on the percentage rejection data with pure solutes and is shown in Fig. 6 (Table 4).

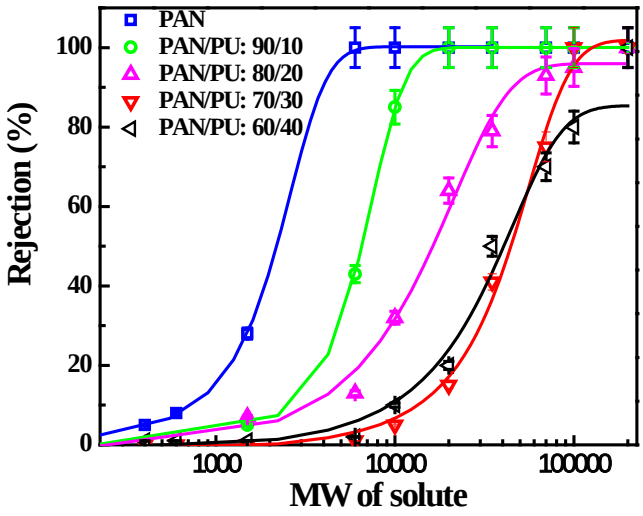

Fig. 6 Molecular weight cut-off of pure and PAN/PU blended membranes at different blend ratios.

As observed, MWCO increases with PU concentration from 4 kDa (PAN) to 14 kDa, 46 kDa, 87 kDa and 128 kDa for various PAN/PU blend ratios of 90/10, 80/20, 70/30 and 60/40, respectively. As reflected from SEM images (Fig. 3), membrane permeability (Fig. 4) and porosity (Fig. 5) increase with PU addition in PAN/PU blend. Highly porous membrane offers lower solute rejection and hence higher MWCO. Thus, at higher PU concentration of 40 wt% in PAN/PU blend, a more porous membrane with higher MWCO of 128 kDa is obtained. But, for pure PAN lowest MWCO (compared to its counter membranes) of 4 kDa is obtained due to its dense and thicker membrane morphology.

3.7 Measurement of average pore size

Average pore diameter of each membrane was calculated using Eq. (6) and BET measurements as well, and the values are reported in Table 4. As observed from Table 4, average pore diameter increases with the addition of PU in PAN/PU blend. Average pore diameter increases from 3.4 nm (pure PAN) to 20.7 nm for PAN/PU blend ratio 60/40. SEM image (Fig. 3) corroborate the above findings very well. With the addition of PU, large sized pores are observed in the membrane skin layer increasing the average pore size of membranes. The permeability as well as membrane porosity increases accordingly.[52] The average pore size from BET result differs slightly from the calculated results obtained using Eq. (6). The average pore diameter determined in Eq. (6), is based on the available through

pores across the cross section of the membrane. BET measurement on the other hand, accounts both through pores as well as blind pores. Hence higher pore sizes are obtained from BET analysis. This discrepancy is notable at lower MWCO and becomes insignificant for higher cut-off membranes (Table 4).

3.8 AFM analysis of membranes

AFM images of the pure PAN and PAN/PU blend membranes are presented in Fig. 7. Dark and light portions in these images indicate the presence of membrane pores and valleys. As shown in Fig. 7, for pure PAN, smooth membrane surface is obtained. The RMS roughness of the membrane was found to be 10 nm (Fig. 7a). With increase in PU concentration in the blend the RMS roughness increases. The roughness of PAN/PU blend membrane followed the order, 90/10 < 80/20 < 70/30 < 60/40 presented in Fig. 7(b) to 7(d). Highest roughness of 200 nm was obtained for 60/40 blend membrane. This can be explained by SEM images (Fig. 3) and the supplementary figure (Fig. S1) that, addition of hydrophilic PU concentration increases the available number of pores as well as their sizes and higher porosity (Fig. 5), in the membrane matrix. Increase in porosity imparts enhanced membrane roughness as shown by AFM images. The results are consistent with the study by Sadeghi et al.,[53] for PES/PVP system.

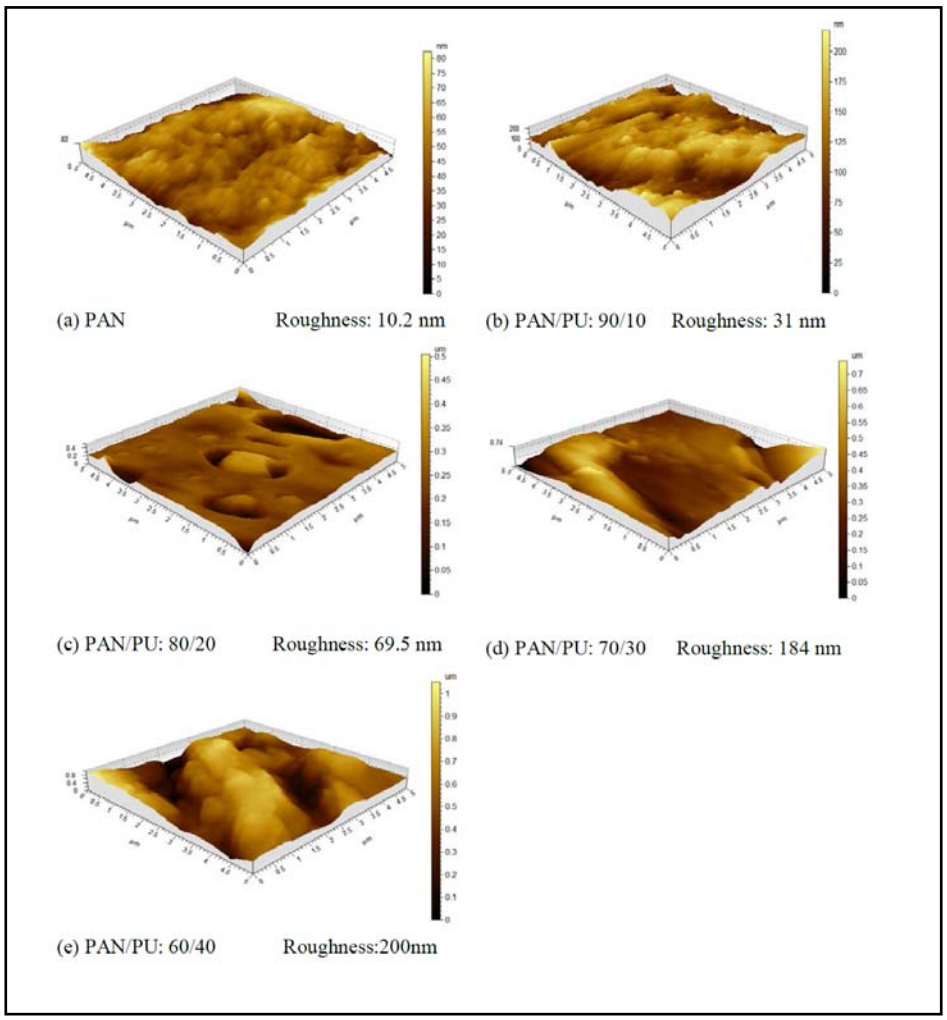

Fig. 7 Root mean surface roughness of pure and blended PAN/PU membranes of various blend ratios (a) PAN (b) 90/10 (c) 80/20 (d) 70/30 (e) 60/40.

3.9 FTIR analysis of PAN/PEG blend membranes

The FTIR ($C \equiv N$) spectra of PAN, PU and PAN/PU blend membranes are shown in Fig. 8. The spectrum of pure PAN membrane shows the transmission band at 2237cm^{-1} confirming the presence of nitrile groups (Fig. 8a).[42] In addition, PAN/PU blend membranes show some notable interactions that reveal structural changes due to the stretching vibration of above functional groups. The stretching frequency of pure PAN membrane at 2237 cm^{-1} is reduced slightly for PAN/PU blend at 90/10, shown in Fig. 8(b). Whereas, its intensity vanishes at higher blend composition of PU i.e., 70/30 and 60/40 membranes (Figs. 8c and 8d). Pure PU membrane (Fig. 8e) shows a characteristic band at 3371 cm^{-1} representing the (–N-H) stretching vibration of urethane group and the corresponding band at 1533 cm^{-1} and 1310 cm^{-1} indicating amide band and (–OCONH-) asymmetric stretching vibrations.[2,3]

Free carbonyl groups (C=O) corresponding to polyester chain and urethane groups are at 1731 cm^{-1} and 1645 cm^{-1}, respectively. The peak at 2948 cm^{-1} highlights the asymmetric stretching vibration of (CH_2) group of polyurethane. Whereas, the peak at 1645 cm^{-1} represents the presence of stretching vibration (C=C) of the aromatic ring.[39] In addition, the stretching frequency due to (N-H) stretching at 3371 cm^{-1} in PU membrane is shifted to 3319 cm^{-1}, 3283 cm^{-1} and 3271 cm^{-1} for different PAN/PU blend ratios highlighted in Figs. 8(b) to 8(d). This shifting of functional groups establishes an interaction between the (N-H) group of urethane and carbonyl groups of PAN. Similar type of shifting of peak is reported by the earlier studies for blend membranes of PAN/Carboxylated polyether imide (CPEI) blend, CA/PU blend.[54,36] This result establishes better compatibility between individual polymers.[55]

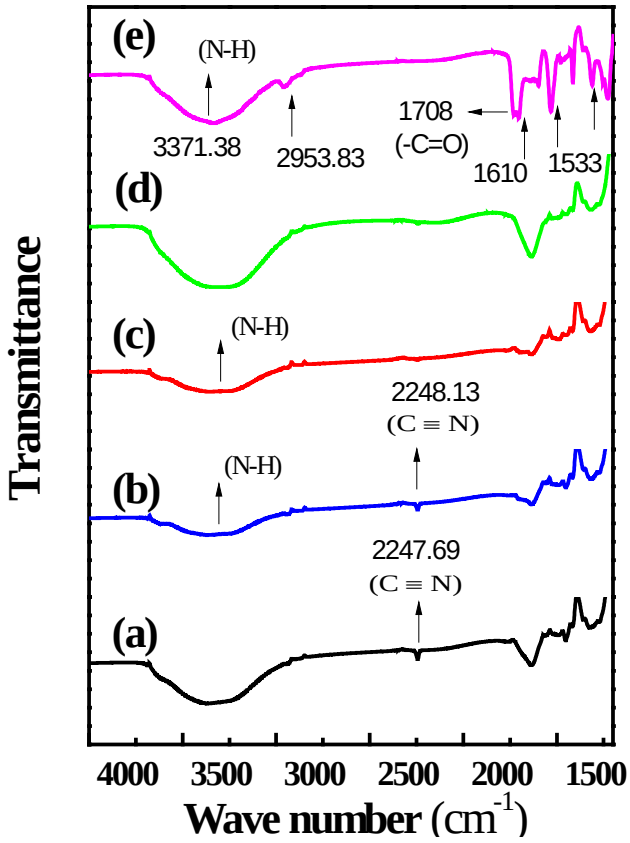

Fig. 8 FTIR spectra of pure and PAN/PU blend membranes (a) PAN (b) PAN/PU: 90/10 (c) PAN/PU: 70/30 (d) PAN/PU: 60/40 (e) PU.

3.10 DSC analysis of PAN/PU blend membranes

The polymer compatibility of blend membrane was confirmed from differential calorimetric (DSC) analysis. The resultant thermograms of pure, as well as PAN/PU blend membranes are shown in the Fig. 9.

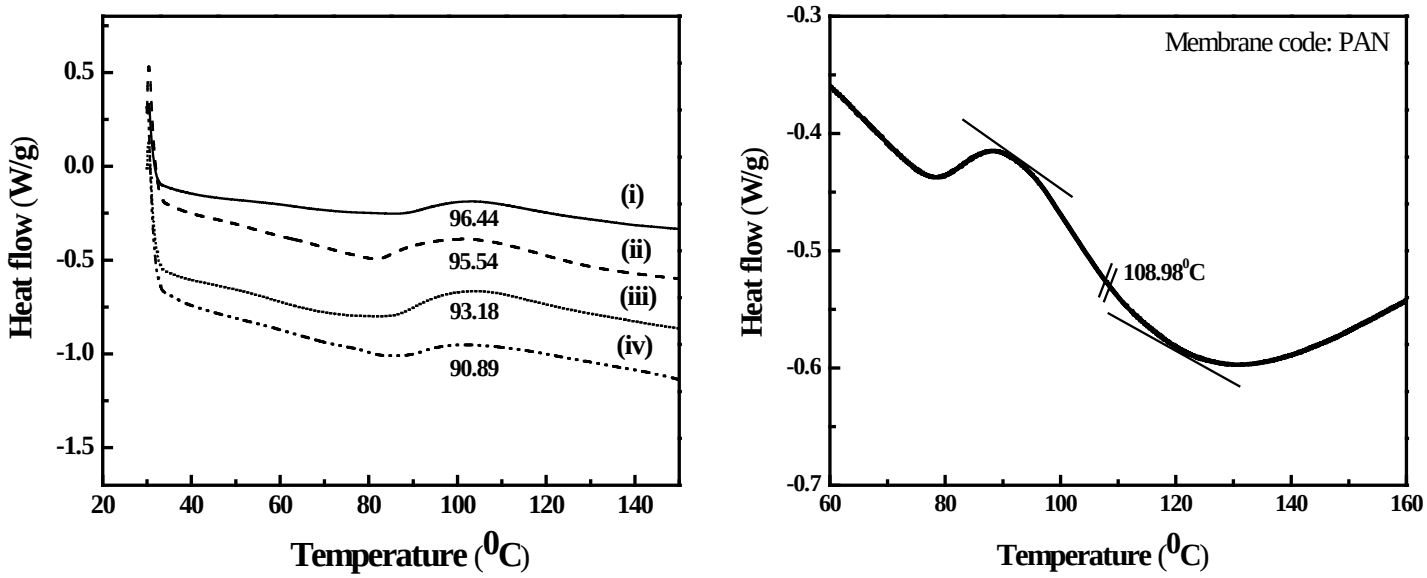

(a) (b)

Fig. 9 Differential scanning calorimetric (DSC) curves for pure and PAN/PU blend membranes (w/w); (a) Effect of blend composition; (i) 90/10 (ii) 80/20 (iii) 70/30 (iv) 60/40; (b) PAN only.

Thermal analysis of membranes using DSC is a valuable tool, as the (theoretical) glass transition temperature difference between PAN and PU exceeds 20 ^{0}C. Experimental determination of T_g value for pure PAN and PU membranes are found to be 108 ^{0}C and 82.97 ^{0}C, which is close to the value reported in literature.[54,56] For blend membranes, glass transition temperatures are found to be 96.44 ^{0}C for 90/10 PAN/PU blend, 95.54 ^{0}C, for 80/20 PAN/PU blend, 93.18 ^{0}C for 70/30 PAN/PU blend and 90.89 ^{0}C for 60/40 PAN/PU blend, respectively at increased PU concentration of 10, 20, 30 and 40 wt%. From the above findings we can interpret that (i) the blend membranes show a single glass transition temperature indicating better compatibility of polymers; (ii) the interaction between polymers decreases with PU concentration; (iii) thermoplastic PU with lower T_g value (compared to PAN) of 82.97 ^{0}C greatly contributes to the decrement in T_g values of

polymeric blend. Presence of PU in PAN inherently increases the chain movement of the blend polymer, as discussed in section 3.1 and 3.2 (Table 3 and Table 4). In addition, earlier reports suggest, membrane having lower glass transition temperature is associated with a loose structure having larger fractional free volume within the matrix.[57] Hence, the lowest T_g, 90.89 ^{0}C is obtained for 60/40 blend composition. These findings corroborate with SEM images and the porosity values presented in the preceding sections. Similar observation is reported by the earlier researcher Barroso et al.,[57] which describe the effect of glycol additive on cellulose acetate/zinc oxide blend membranes.

3.11 Mechanical property analysis

Fig. 10 shows the tensile property of PAN and PAN/PU blend membranes. The figure reveals that, PAN membrane has the highest tensile strength of 23.5 MPa and it decreases to other blend membranes. This can be explained by the morphological behavior of all membranes presented in SEM images (Fig. 3). As the membrane becomes porous, breaking stress decreases as expected. The elongation percentage of the blend membranes increased proportionally with PU concentration. This may be due to the presence of PU, a thermoplastic elastomer. The aliphatic chains contributes to higher tensile strength whereas, cohesive force and intermolecular hydrogen bonding (Fig. 1(b), are responsible for higher elongation percentage of the membrane matrix.[58] Young's modulus of membrane was used to quantify membrane stiffness. PAN membrane exerted the highest modulus 719±22 MPa, compared to 80/20, 70/30 and 60/40 blend compositions having a modulus of 591±55, 455±10 and 398±29 MPa, respectively. To the best of our knowledge, mechanical property of PAN/PU blend membranes has never been reported earlier. However, similar trend of decrease in elastic modulus with membrane porosity is reported with the PAN/PAN-g-PEO blend membranes by Barroso et al.[57]

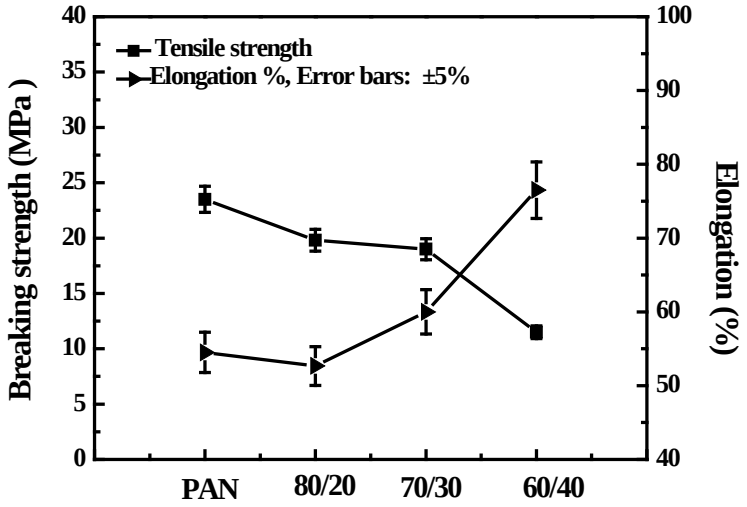

Fig. 10 Tensile strength and percentage elongation of PAN and PAN/PU blend membranes.

3.12 Antifouling property of membrane

The flux decline profiles of PAN and PAN/PU blend membranes are presented in Fig. 11(a). It is observed from this figure that the throughputs of these membranes are according to their permeability values. Corresponding FDR and FRR values are presented in Fig. 11(b).

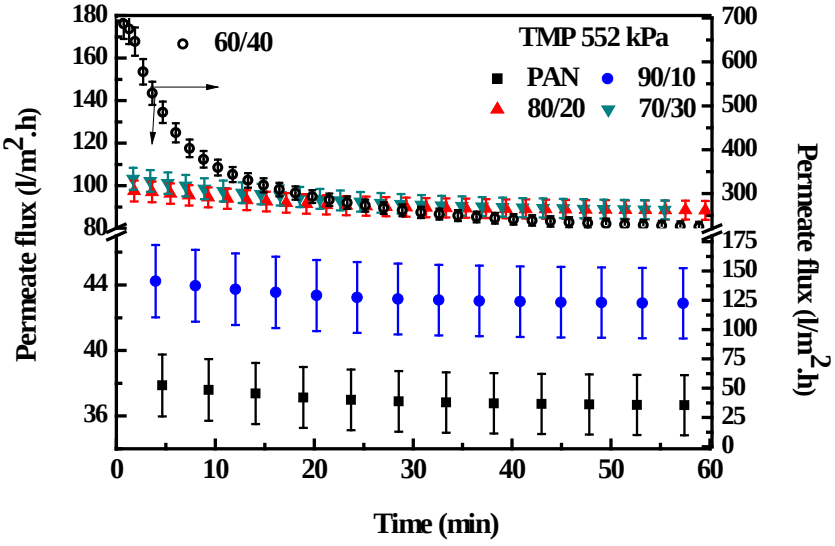

(a)

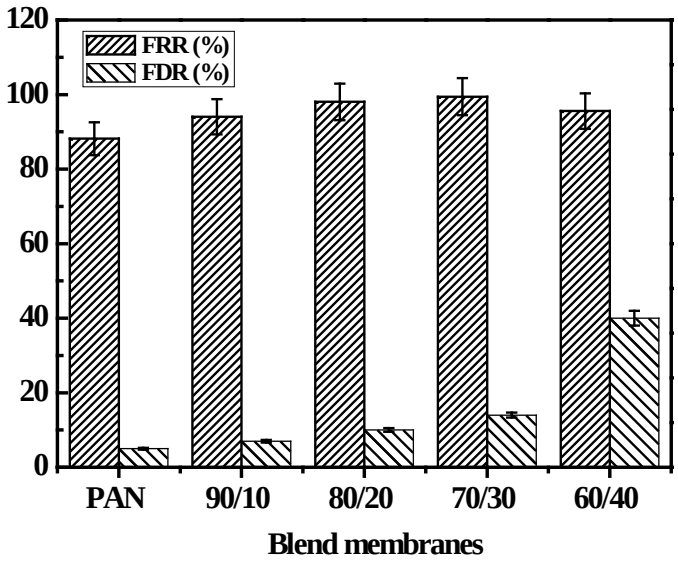

(b)

Fig. 11 Effect of PAN/PU blend ratio on (a) time dependent flux declination with turbid feed of 500 NTU; (b) antifouling parameters FRR and FDR.

It can be observed that FDR values are less than 5% for pure PAN and 90/10 blend membranes. Since, these membranes have the lowest pore size, a fouling layer of solutes are formed over the membrane surface due to concentration polarization leading to sluggish decline in permeate flux. As the membrane become more porous by increasing PU concentration in the blend, two phenomena occur: (i) particles enter into the pore causing pore blocking; (ii) surface roughness of the membranes increases, fouling of the membrane becomes more. These two effects act in tandem leading to more flux decline. Consequently, FDR for 80/20, 70/30 and 60/40 membranes increase in that order as 10, 18 and 40%, respectively. FRR of pure PAN membrane was the lowest (88%). It increases with PU concentration in the blend and for 70/30 PAN/PU blend, FRR was the maximum 99%. This is due to increase in hydrophilicity of these membranes with PU concentration. Chen et al., reported upto 90% FRR using PVDF-microgel blend membranes.[59] Kim et al., showed improved anti-biofouling properties of poly(vinyl alcohol) (PVA) coated, carbon nanotube (CNT) deposited polyamide based reverse osmosis (RO) membranes.[60] Qualitative analysis of feed and permeate after filtration with 500 NTU turbid feed by all set of membranes was carried out and the values are reported in Table 5.

Table 5 Qualitative analysis of feed and permeate after filtration experiment with turbid feed (500 NTU) using PAN/PU blend membranes.

Properties	**Feed**	**Permeate**				
		Control membrane	**PAN/PU blend ratio**			
***Membrane code**		**100/0 (PAN)**	**90/10**	**80/20**	**70/30**	**60/40**
pH	7.4	7.1	7.2	7.2	7.1	7.3
Turbidity (NTU)	500	0	0	0	0	0
Conductivity (µS/cm)	313	309	311	310	312	313
Absorbance at 254 nm	2.7	0.001	0.003	0.019	0.0318	0.0553

*Membrane codes correspond to the composition presented in Table 2.

Complete removal of turbidity and up to 99% of organic substances removal was attained by the blend membranes. The conductivity value for the feed and permeate remain unchanged as membranes are in UF range.

4.0 Conclusion

Preparation, characterization and application of PAN/PU blend membranes are reported in this work. Following are the major conclusions:

(i) Inclusion of PU made the membrane more porous and permeability of the membrane increased from 2×10^{-11} m/Pa.s to 48×10^{-11} for 60/40 PAN/PU blend membranes.

(ii) MWCO of membranes also increased from 4 kDa to 128 kDa for 60/40 PAN/PU blend. Various membranes of intermediate MWCO 14, 46 and 87 kDa were obtained for 90/10, 80/20 and 70/30 blend compositions.

(iii) PU made the membrane more hydrophilic and contact angle was reduced from 76^0 to 52^0 for 60/40 blend membrane.

(iv) Surface roughness of the membrane increased with PU concentration in the blend, made them more prone to fouling.

(v) DSC measurements showed good compatibility between PAN and PU membranes.

(vi) Experiments with turbid water showed that, turbidity and organic concentration in feed water were removed completely by the membranes. PAN/PU 70/30 blend membrane had the maximum antifouling characteristics.

Acknowledgement

This work is partially supported by a Grant from the Board of Research in Nuclear Sciences, Department of Atomic Energy, Government of India, Mumbai, under the scheme no. 2012/2/03-BRNS, Dt. 25-07-2012. Any opinions, findings and conclusions expressed in this paper are those of the authors and do not necessarily reflect the views of BRNS.

Nomenclature

A	Membrane surface area, m^2
C_0	Concentration of feed (mg/l)
C_p	Concentration of permeate (mg/l)
J_p^0, J_p^t	Initial and final permeate flux at the end of time, t (1 hr), $l/m^2.h$
J_w, J_{w1}	Pure water flux of membrane before and after experimental run, $l/m^2.h$
μ	Viscosity of water, Pa.s
ΔP	Transmembrane pressure drop, kPa
R	Rejection, %
Δt	Sampling time, s
r_s	Average pore radius (nm)

Abbreviation

AFM	Atomic force microscopy
CA	Cellulose acetate
CSA	Camphor sulfonic acid
CPEI	Carboxylated polyether imide
CPSF	Carboxylated polysulfone
DSC	Differential scanning calorimetry
DMF	Dimethylformamide

DMAc	Dimethyl acetamide
FRR	Flux recovery ratio
FDR	Flux decline ratio
FTIR	Fourier transform infrared
IPN	Interpenetrating polymer network
MWCO	Molecular weight cut-off
nm	Nanometre
PAN	Polyacrylonitrile
PAM	Polyacrylamide
PANI	Polyaniline
pTSA	p-toluene sulfonic acid
PE	Polyethylene
PEG	Polyethylene glycol
PES	Polyethersulfone
PP	Polypropylene
PSF	Polysulfone
PU	Polyurethane
PVDF	Polyvinylidene fluoride
PVP	polyvinylpyrrolidone
SEM	Scanning electron microscopy
TPU	Thermoplastic polyurethane
UF	Ultrafiltration

References:

1 E. A. Collins, J. Bares and F. W. Jr. Billmeyer, *Experiments in Polymer Science*, Wiley, 1973.

2 I. Yilgor and E. Yilgor, *Polymer*, 1999, **40,** 5575.

3 J. Brandrup, E. H. Immergut, E. A. Grulke, A. Abe and D. R. Bloch, *Polymer Handbook*, Wiley, 1999.

4 L. Lin, Y. Kong, K. Xie, F. Lua, R. Liu, L. Guo, S. Shao, J. Yang, D. Shi and Y. Zhang, *Sep. Purif. Technol*., 2008, **61,** 293.

5 B. K. K. Swamya and Siddaramaiah, *J. Hazard. Mater*., 2003, **B99,** 177.

6 Z. F. Wang, B. Wang, X. M. Ding, M. Zhang, L. M. Liu, N. Qi and J. L. Hu, *J. Membr. Sci*., 2004, **241**, 355.

7 M. Mandru, C. Ciobanu, M. E. Ignat, M. Popa, L. Verestiuc and S. Vlad, *Dig. J. Nananomater Bios*, 2011, **6(3),** 1227.

8 M. Mandru, C. Ciobanu, S. Vlad, M. Butnaru, L. Lebrun and M. Popa, *Cent. Eur. J. Chem.*, 2013, **11(4),** 542.

9 L. A. Utracki, *Polymer Blends Handbook*, Kluwer Academic pub, 2002.

10 M. Liu, C. Xiao and X. Hu, *Desalination*, 2011, **275**, 133.

11 H. Liu, C. Xiao, X. Hu and M. Liu, *J. Membr. Sci*., 2013, **427**, 326.

12 X. Zhao, H. Zhang and J. Wang, *Chin. J. Chem. Eng*, 2014, **22(5),** 583.

13 G. Ciobanu, G. Carja and O. Ciobanu, *Desalination*, 2008, **222**, 197.

14 H. R. Pant, H. J. Kim, M. K. Joshi, B. Pant, C. H. Park, J. I. Kim, K. S. Huid and C. S. Kim, *J. Hazard. Mater*., 2014, **264**, 25.

15 M. A. Frommer and R. M. Massalem, *Ind. Eng. Chem. Prod. Res. Develop*, 1993, **12(4)** 328.

16 Z. S. Petrovic, Z. Zavargo, J. H. Fly and W. J. Macknight, *J. Appl. Polym. Sci*., 1994, **51**, 1087.

17 K. Rzeszutek and A. Chow, *J. Membr. Sci*., 2001, **181**, 265.

18 L. I. B. David and A. F. Ismail, *J. Membr. Sci*., 2003, **213**, 285.

19 I. C. Kim, H. G. Yun and K. H. Lee, *J. Membr. Sci*., 2002, **199**, 75.

20 N. Scharnagl and H. Buschatz, *Desalination,* 2001, **139**, 191.

21 E. R. Cornelissen, T. V. Boomgaard and H. Strathmann, *Colloids Surf. A: Physico chem. Eng. Aspects*, 1998, **138**, 283.

22 Q. Zhou, L. Zhang and M. Zhang, *Polymer*, 2003, **44**, 1733.

23 M. Sivakumar, D. Mohan and R. Rangarajan, *Part 1. Polym. International*, 1998, **47**, 311.

24 M. sivakumar, R. Malaisamya, C. J. Sajitha, D. Mohan, V. Mohana and R. Rangarajan, *Eur. Polym. J.*, 1999, **35**, 1647.

25 M. Sivakumar, D. Mohan and R. Rangarajan, *J. Membr. Sci*., 2000, **169**, 215.

26 P. D. Nair, M. Jayabalam and V. N. Krishramurthy, *J. Polym. Sci. Part A: Polym. Chem.*, 1990, **28**, 3775.

27 R. Malaisamy, D. R. Mohan and M. Rajendran, *J. Colloid Interface Sci*., 2002, **254**, 129.

28 C. S. Latha, D. Shanthanalakshmi, D. Mohan, K. Balu and M. D. K. Kumarasamy, *J Appl. Polym. Sci.*, 2005, **97**, 1307.

29 Z. Yuan and X. Dan-Li, *Desalination*, 2008, **223**, 438.

30 F. D. R. Amado, L. F. Rodrigues Jr., M. A. S. Rodrigues, A. M. Bernardes, J. Z. Ferreira and C. A. Ferreira, *Desalination*, 2005, **186,** 199–206.

31 D. Zavastin, I. Cretescu, M. Bezdadea, M. Bourceanu, M. Dragan, G. Lisa, I. Mangalagiu, V. Vasic and J. Savic, *Colloids and Surfaces A: Physicochem. Eng. Aspects*, 2010, **370**, 120.

32 S. Velu, L. Muruganandam and G. Arthanareeswaran, *Int. J. Chem. Anal. Sci.,* 2011, **2(7)**, 87.

33 Y. Wu, G. Tian, H. Tan and X. Fu, *Desalination and Water Treatment*, 2013, **51**, 5311.

34 M. Tijink, J. Janssen, M. Timmer, J. Austen, Y. Aldenhoff, J. Kooman, L. Koole, J. Damoiseaux, R. van Oerle, Y. Henskensh and D. Stamatialis, *J. Mater. Chem. B*, 2013, **1**, 6066.

35 C. Nie, L. Ma, Y. Xia, C. He, J. Deng, L. Wang, C. Cheng, S. Sun and C. Zhao, *J. Membr. Sci.,* 2015, **475**, 455.

36 C. Cheng, S. Sun and C. Zhao, *J. Mater. Chem. B*, 2014, **2**, 7649.

37 Z. Yin, C. Cheng, H. Qin, C. Nie, C. He and C. Zhao, *J Biomed Mater Res Part B*, 2015, **103**, 97.

38 A. Roy, P. Dadhich, S. Dhara and S. De, RSC *Adv.*, 2015, **5**, 7023.

39 J. Wijmans, J. Kant, M. Mulder and C. Smolders, *Polymer*, 1985, **26**, 1539.

40 P. Rai, G. C. Majumdar, S. DasGupta and S. De, *Food Sci. and Technol.,* 2007, **40**, 1765.

41 S. R. Panda, S. De, *Polym. Eng. Sci.,* 2014, **54(10),** 2375.

42 S. Singh, K. C. Khulbe, T. Matsuuraa and P. Ramamurthy, *J. Membr. Sci*., 1998, **142**, 111.

43 R. Guan, H. Dai, C. Li, J. Liu and J. Xu, *J. Membr. Sci*., 2006, **277**, 148.

44 S. R. Panda and S. De, *J. Polym. Res.,* 2013, **20**, 179.

45 S. T. Kao, M. Y. Teng, C. L. Li, C. Y. Kuo, C. Y. Hsieh, H. A. Tsai, D. M. Wang, K. R. Lee and J. Y. Lai, *Desalination*, 2008, **233**, 96.

46 M. Sadrzadeh and S. Bhattacharjee, *J. Membr. Sci*., 2013, **441**, 31.

47 L. Tan, D. Pan and N. Pan, *J. Appl. Polym. Sci.*, 2008, **110**, 3439.

48 Y. D. Kim, J. Y. Kim, H. K. Lee and S. C. Kim, *J. Appl. Polym. Sci.*, 1999, **73**, 2377.

49 Z. Wang, J. Ma and Q. Liu, *Desalination*, 2011, **278,** 141.

50 E. Saljoughi, M. Amirilargani and T. Mohammadi, *Desalination*, 2010, **262**, 72.

51 H. Kumar and Siddaramaiah, *J. Hazard. Mater*., 2007, **148,** 467.

52 D. B. Mosqueda-Jimenez, R. M. Narbaitz, T. Matsura, G. Choudhury, G. Pleizier, J. P. Santerre, *J. Membr. Sci*., 2004, **231**, 209.

53 I. Sadeghi, A. Aroujalian, A. Raisi, B. Dabir and M. Fathizadeh, *J. Membr. Sci.*, 2013, **430**, 24.

54 S. Senthilkumar, S. Rajesh, A. Jayalakshmi and D. Mohan, *Sep. Purif. Technol*., 2013, **107**, 297.

55 A. Litmanovich and N. Plate, *Macromol. Chem. Phys.*, 2000, **201**, 2176.

56 R. Saranya, G. Arthanareeswaran, S. Sakthivelu and P. Manohar, *Ind. Eng. Chem. Res.*, 2012, **51**, 4942.

57 M. Ali, M. Zafar, T. Jamil and M. T. Z. Butt, *Desalination*, 2011, **270**, 98.

58 T. Barroso, M. Temtem, T. Casimiro and A. Aguiar-Ricardo, *J. Supercrit. Fluids*, 2011, **56**, 312.

59 X. Chen, B. Zhao, L. Zhao, S. Bi, P. Han, X. Feng and L. Chen, *RSC Adv*., 2014, **4**, 29933.

60 H. J. Kim, Y. Baek, K. Choi, D. Kim, H. Kang, Y. Choi, J. Yoon and J. Lee, *RSC Adv*., 2014, **4**, 32802.

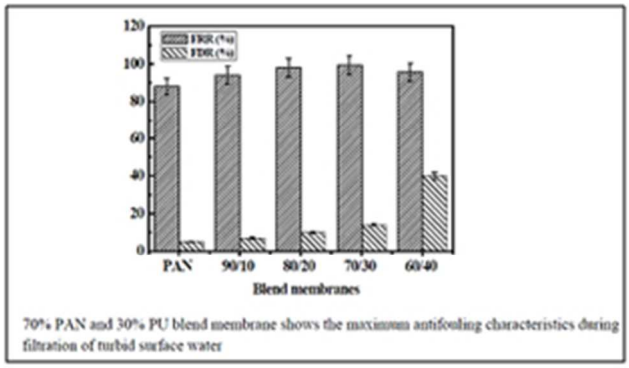

83x49mm (96 x 96 DPI)